



This is the accepted manuscript made available via CHORUS. The article has been published as:

Aqueous harvesting of math
 Zr at a radioactive-ion-
beam facility for cross-section measurements

Jennifer A. Shusterman, Nicholas D. Scielzo, E. Paige Abel, Hannah K. Clause, Nicolas D. Dronchi, Wesley D. Frey, Narek Gharibyan, Jason A. Hart, C. Shaun Loveless, Sean R. McGuinness, Logan T. Sutherlin, Keenan J. Thomas, Suzanne E. Lapi, J. David Robertson, Mark A. Stoyer, Eric B. Norman, Graham F. Peaslee, Gregory W. Severin, and Dawn A. Shaughnessy

Phys. Rev. C **103**, 024614 — Published 26 February 2021

DOI: [10.1103/PhysRevC.103.024614](https://doi.org/10.1103/PhysRevC.103.024614)

Aqueous Harvesting of ^{88}Zr at a Radioactive-Ion-Beam Facility for Cross Section Measurements

Jennifer A. Shusterman,^{1,2} Nicholas D. Scielzo,³ E. Paige Abel,^{4,5} Hannah K. Clause,^{4,5} Nicolas D. Dronchi,⁴ Wesley D. Frey,⁶ Narek Gharibyan,³ Jason A. Hart,⁴ C. Shaun Loveless,⁷ Sean R. McGuinness,⁸ Logan T. Sutherlin,⁹ Keenan J. Thomas,³ Suzanne E. Lapi,⁷ J. David Robertson,⁹ Mark A. Stoyer,³ Eric B. Norman,¹⁰ Graham F. Peaslee,⁸ Gregory W. Severin,^{4,5} and Dawn A. Shaughnessy³

¹*Hunter College of the City University of New York, New York, NY 10065*

²*Graduate Center of the City University of New York, New York, NY 10016*

³*Lawrence Livermore National Laboratory, Livermore, CA 94550*

⁴*Michigan State University, East Lansing, MI 48824*

⁵*National Superconducting Cyclotron Laboratory, East Lansing, MI 48824*

⁶*McClellan Nuclear Research Center-UC Davis, McClellan, CA 95652*

⁷*University of Alabama at Birmingham, Birmingham, AL 35294*

⁸*University of Notre Dame, Notre Dame, IN 46556*

⁹*University of Missouri, Columbia, Columbia, MO 65211*

¹⁰*University of California, Berkeley, Berkeley, CA 94720*

(Dated: February 2, 2021)

Isotope harvesting is a method of collecting the long-lived radioisotopes that build up during the operation of ion-beam facilities in a way that is useful for subsequent research. As a demonstration of this method for the collection of a Group IV metal at a fragmentation facility, the high-energy ^{88}Zr secondary beam produced from a 140-MeV/u ^{92}Mo primary beam at the National Superconducting Cyclotron Laboratory (NSCL) was stopped in a water target. The setup aimed to mimic the aqueous beam dump that will be implemented at the Facility for Rare Isotope Beams (FRIB). The collected ^{88}Zr and accompanying ^{88}Y decay daughter were radiochemically extracted from the solution and made into target samples suitable for neutron-capture cross-section measurements. These samples were then irradiated at two reactor facilities, and the ^{88}Zr average thermal-neutron-capture cross section (σ_T) and resonance integral (I) were determined to be $\sigma_T = (8.04 \pm 0.63) \times 10^5$ b and $I = (2.53 \pm 0.28) \times 10^6$ b. The σ_T value agrees well with previous results and I , determined for the first time here, was found to be the largest measured resonance integral by two orders of magnitude. The ^{88}Y thermal-neutron-capture cross section was determined to be less than 1.8×10^4 b. This work demonstrates the steps needed to make cross-section measurements with samples produced via aqueous isotope harvesting.

I. INTRODUCTION

Long-lived radionuclides are produced and accumulate at various locations within an accelerator during routine operation. Isotope harvesting [1] is the collection and purification of these byproduct radionuclides for use in subsequent research. Initial uses of this method have shown great promise to complement the conventional methodologies. At the Paul Scherrer Institute (PSI) in Switzerland, the copper beam dump that had been used during high-energy proton irradiations was dissolved, and the ^{60}Fe ($t_{1/2} = 2.62 \times 10^6$ yr) present was radiochemically separated from the mixture. A sufficiently pure amount of ^{60}Fe was isolated [2] to measure its half-life [3–5] and neutron-capture cross section [6, 7], and to produce a set of standards for accelerator mass spectrometry [8]. In addition, numerous other isotopes are being pursued from the copper beam dump [9], irradiated graphite targets [10], and stainless steel parts [11] at PSI.

The implementation of isotope harvesting at the upcoming Facility for Rare Isotope Beams (FRIB) at Michigan State University (MSU) has attracted considerable interest because of the large quantities of a broad range of radioisotopes that will be produced during routine op-

eration. At FRIB, a water-filled beam dump will be utilized to stop the primary beam and much of the beam-fragment distribution, opening up new opportunities to collect radioisotopes sought after in areas of nuclear science ranging from national security to medicine. Thus, in preparation for an extensive isotope-harvesting program at FRIB, there have been several efforts to investigate the efficacy of extracting radioisotopes deposited in a water target [12–16].

Initial efforts at the National Superconducting Cyclotron Laboratory (NSCL), which produces radioisotopes using the same fragmentation process as at FRIB, albeit at significantly lower intensities, demonstrated the successful recovery of ^{24}Na and ^{67}Cu from an aqueous target [12–14]. Both sodium and copper are well suited for collection and extraction from an aqueous environment—these elements have well understood redox and speciation chemistry in near neutral environments, only exist as monovalent and divalent cations in solution, and do not hydrolyze irreversibly.

Other elements, such as Zr, V, and Hf, present challenges. These group IV and V metals tend to exist in tetravalent and pentavalent oxidation states, and form oxide and hydroxide complexes in aqueous conditions

that are not highly acidic. This effect is most pronounced when metal concentrations exceed the micromolar regime [17]; however, even at trace concentrations, such as those expected for radioisotopes, mononuclear hydroxide complexes can form. Recent results have indicated a reduced recovery efficiency for ^{48}V deposited in an aqueous solution at the NSCL, potentially due to redox and radiolysis chemistry [15]. The work presented here is the first aqueous harvesting collection of a group IV element, and the efficacy of the method for collection of a hydrolyzable metal is assessed.

Several radioactive Zr isotopes are valuable to nuclear science, including ^{86}Zr and ^{89}Zr for nuclear medicine [18, 19], ^{95}Zr for astrophysics [20], and ^{88}Zr and ^{89}Zr for stockpile-stewardship applications. For example, ^{88}Zr is part of a neutron-induced reaction network that is of interest for interpreting data from radiochemical detectors used in underground nuclear tests [21]. The daughter of ^{88}Zr , ^{88}Y , is also part of this network as well as of interest to the astrophysical community for p -process investigations [22]. Analysis of historic test data using such cross sections is an aspect of the United States Science-Based Stockpile Stewardship Program, which aims to provide high confidence in the safety, security, reliability, and effectiveness of the nuclear stockpile without nuclear testing [23]. The only measurements of a neutron-induced reaction on ^{88}Zr were of the $^{88}\text{Zr}(n,2n)^{87}\text{Zr}$ cross section at 14.8 MeV [24] and the thermal neutron-capture cross section on ^{88}Zr recently measured using samples produced via the $^{89}\text{Y}(p,2n)^{88}\text{Zr}$ reaction. The latter result revealed that the thermal-neutron-capture cross section on ^{88}Zr is $(8.61 \pm 0.69) \times 10^5$ b, which is the second largest reported neutron-capture cross section [25]. Similarly, the $^{88}\text{Y}(n,2n)^{87}\text{Y}$ was measured at 14.8 MeV [24], and recent efforts have aimed to constrain the neutron-capture cross section on ^{88}Y from 0.01 to 1 MeV using the Oslo Method [22].

In the work presented here, a secondary beam of ^{88}Zr was collected in the water target irradiation cell of an aqueous harvesting endstation [12] at the NSCL in a dedicated experiment. While most harvesting efforts at FRIB will be carried out continuously without interfering with a users experiment, dedicated experiments for proof-of-concept work at NSCL are useful to validate methodologies for both production and separation. The steps needed to extract and purify the ^{88}Zr produced via aqueous harvesting for a subsequent neutron-capture cross-section measurement were demonstrated. The aqueous samples were subsequently shipped to Lawrence Livermore National Laboratory (LLNL) for radiochemical separations and preparation of ^{88}Zr and ^{88}Y targets for measurements of thermal-neutron-capture cross sections. The targets were irradiated at two nuclear reactors, the University of Missouri Research Reactor (MURR) and the McClellan Nuclear Research Center (MNRC), to perform measurements of the neutron-capture cross sections. The measurements served to reproduce the recent ^{88}Zr neutron-capture results [25] and to better discern the

relative contribution of thermal versus resonance region neutrons. While aqueous harvesting efforts at the NSCL have successfully demonstrated collection and purification of several radionuclides [12–15], the present effort is the first to utilize an aqueous harvested radionuclide for a subsequent measurement.

The methods developed for purifying Zr from the co-produced fragmentation products and harvesting matrix can be adapted to yield multiple useful samples once FRIB is online. Based on the expected production rates at FRIB, approximately 630 mCi of ^{88}Zr ($t_{1/2} = 83.4$ d) will be made per week running with a full-intensity ^{92}Mo primary beam [1]. Given the notoriously complex speciation of Zr at near-neutral pH [26] and irradiation restrictions (e.g. minimal organic content and residual fluoride) on the final ^{88}Zr target material, the efficacy and efficiency of Zr recovery chemistry post-aqueous harvesting is important to assess.

II. AQUEOUS ISOTOPE HARVESTING OF ^{88}Zr AT NSCL

At the NSCL, a 10-pnA, 140-MeV/u ^{92}Mo primary beam impinged upon a 446-mg/cm² beryllium target to produce a range of fragmentation products. The A1900 projectile-fragment separator [27, 28] was used to select the ^{88}Zr secondary beam for delivery to the irradiation cell. The overall beam composition was measured periodically throughout the run at the A1900 via the particle identification detector (PID), which characterizes the beam components by energy-loss and time-of-flight measurements of the individual ions. By adjusting the settings of the dipole magnets and mass slits of the separator, a momentum acceptance of 1.36% was achieved, which yielded the typical beam composition summarized in Table I.

The beam current was continuously measured using a non-intercepting beam monitor which provided a signal proportional to the electromagnetic field produced by the beam. To normalize this signal, direct measurements of the beam current were obtained regularly throughout the run both from a Faraday cup (FC), briefly inserted into the beam path immediately upstream of the endstation, and from the activity deposited in a graphite puck, positioned in front of the irradiation cell window for 5 minutes between each water target irradiation. The radioactive species collected in these $\frac{1}{2}$ -inch-thick graphite pucks were quantified within 1 hour using a high-purity germanium (HPGe) γ -ray detector. It was assumed that the activities in the puck were representative of the beam composition and that nuclear reactions with the carbon did not substantially contribute to the observed products. The radionuclides detected in the puck are compared in Table I to the distribution of isotopes detected at the A1900. These two diagnostics indicated that ^{88}Zr was the most prevalent species in the beam, and overall gave consistent results, although the stable isotopes could not

TABLE I. Beam composition observed at the A1900 Particle Identification Detector and in the graphite puck. The radionuclide composition of the beam in the puck was determined from the emitted γ -rays after a 5-min irradiation. The rates in atoms/sec were inferred from the observed activities, after correcting for decay losses, and accounting for the puck irradiation time. For both the PID and the puck, the intensity of each radionuclide has also been listed normalized to ^{88}Zr .

Nuclide	Half-Life	PID Atom %	Puck (atoms/sec)	PID Norm. to ^{88}Zr	Puck Norm. to ^{88}Zr
^{91}Nb	680 yr	0.35%	-	0.007	-
^{90}Nb	14.60 h	15.28%	1.28×10^7	0.316	0.394
^{89}Nb	2.03 h	0.20%	-	0.004	-
^{89}Zr	78.41 h	4.76%	3.44×10^6	0.099	0.106
^{88}Zr	83.4 d	48.33%	3.26×10^7	1.000	1.000
^{87}Zr	1.68 h	0.31%	2.26×10^5	0.006	0.007
^{86}Zr	16.5 h	-	9.24×10^4	-	0.003
^{87}Y	79.8 h	14.50% ^a	1.12×10^6	0.300 ^a	0.034
^{87m}Y	13.37 h	-	7.65×10^6	-	0.235
^{86}Y	14.74 h	9.91% ^a	2.44×10^6	0.205 ^a	0.075
^{86m}Y	47.4 min	-	2.23×10^6	-	0.068
^{85}Y	2.68 h	-	3.45×10^5	-	0.011
^{84}Y	39.5 min	-	1.72×10^5	-	0.005
^{86}Sr	Stable	0.32%	-	0.007	-
^{85}Sr	64.849 d	4.94%	-	0.102	-
^{84}Sr	Stable	0.43%	-	0.009	-
^{81}Sr	22.3 min	-	3.69×10^4	-	0.001
^{84}Rb	32.82 d	0.33%	-	0.007	-
^{83}Rb	86.2 d	0.25%	-	0.005	-
^{82}Rb	1.2575 min	0.09%	-	0.002	-
^{81}Rb	4.572 h	-	2.39×10^5	-	0.007

^a The PID did not distinguish between the isomer and ground state, so both contributions are reported as ground state.

be quantified with γ -ray spectroscopy. This beam calibration indicated that the average rate of ^{88}Zr impinging upon the irradiation cell was 1.1×10^7 pps. Therefore, over the course of 6.1 days, $(5.8 \pm 0.4) \times 10^{12}$ atoms (responding to $15.0 \pm 1.0 \mu\text{Ci}$) of ^{88}Zr were delivered to the cell.

The ^{88}Zr beam entered the water-filled irradiation cell by passing through a gold vapor-deposited titanium window. To minimize chemical interactions, the cell walls were made of PEEK and the Au side of the window, which consisted of a $0.15\text{-}\mu\text{m}$ -thick layer of Au on a $75\text{-}\mu\text{m}$ -thick Ti foil, was in contact with the water. Prior to irradiation, the double-distilled water (OmniTrace[®] Ultra) in the irradiation cell was sparged with atmospheric pressure helium gas. After beam was deposited in the irradiation cell for an extended period of time typically ranging from 10-16 hours, the water was transferred to an acid-washed PTFE bottle. Following irradiation, the water was measured to be pH 5; each sample was acidified with 3M HCl to decrease the pH to about 1.5, in an effort to minimize Zr hydrolysis. In total, 10 bottles, each with 100 mL of irradiated water, were collected over the course of the experiment.

After each irradiation, the bottle of water was removed from the endstation and the radioisotope content was analyzed using a HPGe detector in an analogous way as with the pucks. A typical γ -ray spectrum is shown in Fig. 1. The ^{88}Zr activity was characterized with the detection of its characteristic 392.87-keV γ ray (emitted

with a γ -ray intensity $I_\gamma=97.29\%$) [29]. A large number of other radioisotopes were also present in the water sample, with the spectrum dominated by the intense γ rays from the decays of the short-lived products ^{90}Nb and ^{86}Y . Radionuclides detected in the puck were also consistent with those collected in the water samples with the exception of ^{83}Sr , which was only detected in the water, due to its relatively low yield and the short irradiation time for the puck. The presence of 514-keV γ rays emitted following the decay of ^{85}Sr could not be detected in the pucks or the water samples immediately after bombardment because it was obscured by the annihilation radiation, but it was identified once much of the shorter-lived activity contributing to the annihilation peak reduced in intensity after several weeks of decay. The presence of some short-lived activities was reduced in the water relative to the puck as a results of decay during irradiation. The total activity of ^{88}Zr collected in the bottles was $9.6 \pm 0.9 \mu\text{Ci}$ at the end of all the collections, consisting of about 60% of the total ^{88}Zr delivered to the irradiation cell. Eight of the bottles, containing a total activity of $9 \mu\text{Ci}$ of ^{88}Zr , were sent to LLNL for chemical processing. The two bottles from the shortest collections remained at MSU for small-scale chemistry tests.

Following the last collection, the empty irradiation cell was disassembled and the window removed so that the activity retained on these pieces could be assessed. Autoradiography of the cell and window was performed, and the image-plate results following a 16-hour exposure time

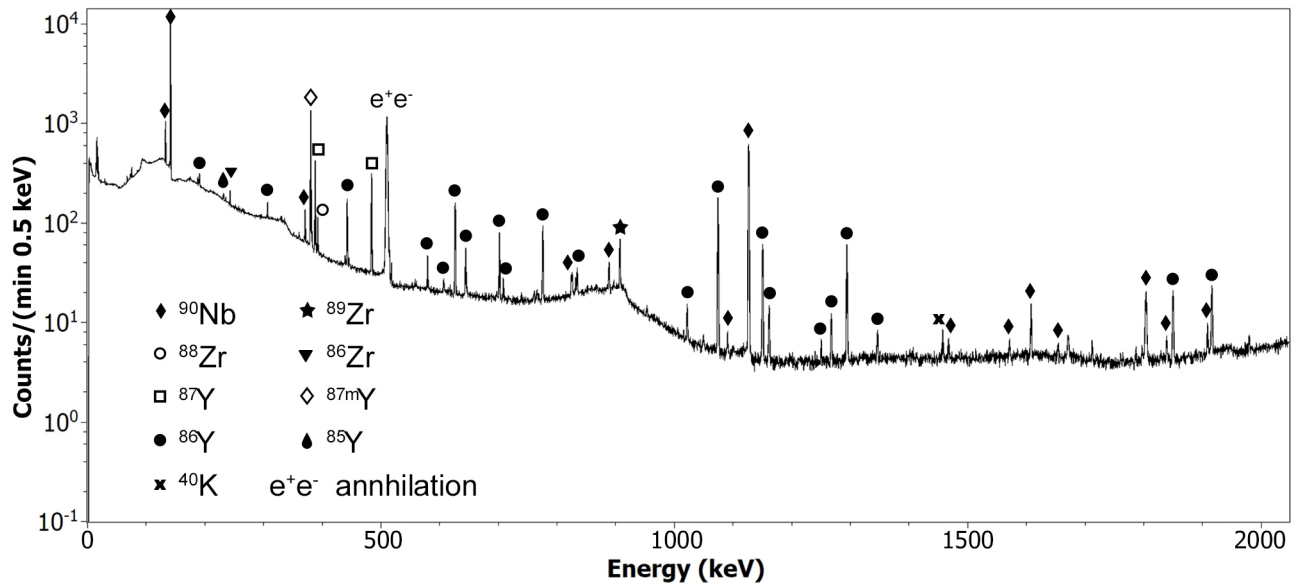


FIG. 1. γ -ray spectrum from a typical bottle containing an aqueous sample recorded 7 hours after being collected at the NSCL. Decay and efficiency corrections have not been applied. In addition to ^{88}Zr , many other ^{92}Mo fragmentation products are observed, including ^{90}Nb , $^{87\text{m}}\text{Y}$, and ^{86}Y .

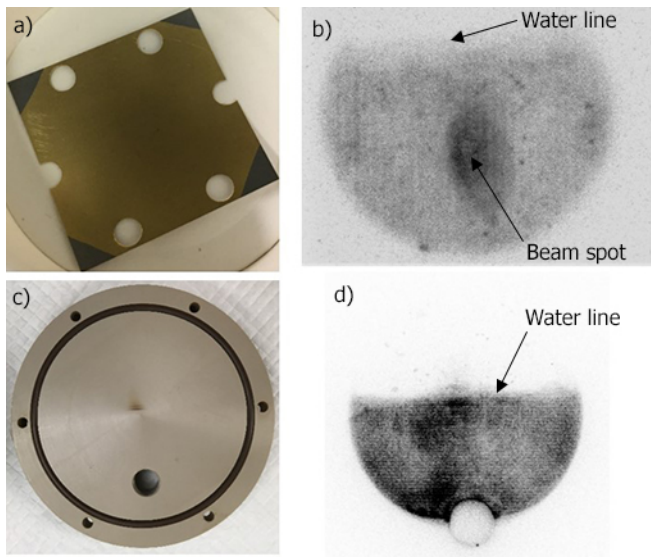


FIG. 2. a) photograph of the gold vapor-deposited titanium entrance window to the cell prior to irradiation, b) autoradiograph of the window after irradiation, c) photograph of the backplate of the cell after irradiation, d) autoradiograph of the backplate of the cell after irradiation. In (b) and (d), the darker areas indicate locations with higher radioactivity. The cell backplate, which was in contact with the water of the cell, contains about 12 times the radioactivity of the entrance window.

where the water had been in contact with the PEEK and splash marks from when the water had been transferred from the cell to the PTFE bottles.

Gamma-ray spectroscopy of the irradiation cell and window indicated that they had about 5.9 ± 0.2 and $0.5 \pm 0.04 \mu\text{Ci}$ of ^{88}Zr adsorbed, respectively. Together, these quantities accounted for the remaining 40% of the delivered ^{88}Zr activity. The ^{88}Zr activity on the backplate is about 12 times that observed on the window; this is not purely due to the surface area exposed to the water, which would account for approximately a factor of 4. It is not clear why the Zr adsorbed to the PEEK to such a high degree, but it is possible that a hydrolyzed Zr species coordinated with the ketone moieties of the PEEK surface. In addition, $^{87/87\text{m}}\text{Y}$, ^{89}Zr , ^{86}Y , and ^{90}Nb were also adsorbed. By the time the spectra were collected on the cell and window, nearly all of the ^{87}Zr ($t_{1/2} = 1.68 \text{ h}$) had decayed to $^{87/87\text{m}}\text{Y}$. It is assumed that the higher localization of $^{87/87\text{m}}\text{Y}$ activity on the cell and window rather than in the water is a result of this decay. This is similarly the case with ^{86}Y , produced from the decay of ^{86}Zr .

III. RADIOCHEMICAL PROCESSING AND TARGET FABRICATION

The 8 bottles received at LLNL had a total of 800 mL of dilute HCl. The radiochemical processing was performed about one month after the sample collection, and at that time the samples contained approximately $7 \mu\text{Ci}$, or 0.4 ng , of ^{88}Zr as well as about $1.1 \mu\text{Ci}$, or 0.1 ng , of ^{88}Y resulting from ^{88}Zr decay. Most of the other radioiso-

are shown in Fig. 2. The autoradiograph of the window shows a clear image of the beam spot as well as where the water had been in contact with the window. The autoradiograph of the backplate of the cell similarly shows

286 topes have half-lives short enough that they had decayed 344
 287 away, with only ^{85}Sr and ^{83}Rb still present in the sample 345
 288 in detectable amounts. Of the 8 bottles, 6 were radio- 346
 289 chemically processed to purify ^{88}Zr and ^{88}Y to serve as 347
 290 target materials for neutron-capture cross section mea- 348
 291 surements. 349

292 The overall chemistry flowsheet used to isolate the ^{88}Y 350
 293 and ^{88}Zr samples is shown in Fig. 3. The ^{88}Y and ^{88}Zr 351
 294 needed to be concentrated into a smaller volume and sep- 352
 295 arated from one another, which was done using cation ex- 353
 296 change and co-precipitation followed by anion exchange, 354
 297 respectively. Previous work successfully demonstrated 355
 298 separations of ^{88}Zr from stable Y target material us- 356
 299 ing anion exchange chromatography [25]. However, as 357
 300 a result of the large volume of solution generated dur- 358
 301 ing aqueous harvesting, a pre-concentration step was re- 359
 302 quired for these samples. Evaporating the water sam- 360
 303 ples for pre-concentration, as had been done in previous 361
 304 aqueous harvesting experiments [12, 15], resulted in ^{88}Zr 362
 305 irreversibly adsorbed to the polypropylene tubes. There- 363
 306 fore, various pre-concentration and separation techniques 364
 307 were tested, with the highest recovery ($\sim 70\%$) coming 365
 308 from co-precipitation of the ^{88}Zr using $\text{La}(\text{OH})_3$ followed 366
 309 by anion exchange. Stable Zr carrier could not be added 367
 310 as this would interfere with the subsequent neutron irra- 368
 311 diation. 369

312 Given the low mass of Zr, co-precipitation with La was 370
 313 done via hydroxide precipitation with NH_4OH , which 371
 314 carries both the Zr and the Y. To minimize the total 372
 315 mass of La introduced, 4 mg of La^{3+} were used by iter- 373
 316 atively co-precipitating 2×20 mL aliquots of the NSCL 374
 317 collections with 1 mg La^{3+} in each tube. The precipi- 375
 318 tated mixture was centrifuged at 4000 rpm for 5 minutes 376
 319 and the supernatant removed. The precipitate was dis- 377
 320 solved in concentrated HCl and the next 20 mL of the 378
 321 sample solution added, repeating the precipitation proce- 379
 322 dure. The supernatants were spiked with an additional 1 380
 323 mg of La carrier and precipitated, centrifuged, and sep- 381
 324 arated again. The precipitates from each of the two passes 382
 325 were dissolved in concentrated HCl and combined. This 383
 326 co-precipitation process successfully concentrated greater 384
 327 than 95% of the ^{88}Zr from the aqueous samples. 385

328 The dissolved $\text{La}(\text{OH})_3$ precipitate from the pre- 386
 329 concentration step was evaporated to wetness and addi- 387
 330 tional concentrated HCl added with a couple of drops of 388
 331 30% unstabilized H_2O_2 ($\sim 50\mu\text{L}$), which helped keep Zr 389
 332 in solution. The stock was heated briefly to destroy the 390
 333 peroxide prior to loading on Dowex 1X8 (100-200 mesh, 391
 334 $1\text{ cm} \times 7\text{ cm}$, column volume (CV) $\approx 5\text{ mL}$) strong-base 392
 335 anion exchange resin that was preconditioned with con- 393
 336 centrated HCl. After adding the loading solution (~ 2.5 394
 337 mL), the resin was washed with 6 CVs of concentrated 395
 338 HCl to elute the Y and La. The Zr was eluted with 2M 396
 339 HCl in 5 CVs. Likely as a result of hydrolysis of the 397
 340 Zr upon stopping in the water during irradiation, it ad- 398
 341 hered to the polypropylene containers used for chemistry, 399
 342 which otherwise would typically have low Zr retention. 400
 343 Desorption of the Zr was attempted with a variety of 401

matrices with the most successful being a mixture of hot
 concentrated HCl and a few drops of 30% unstabilized
 H_2O_2 , added to the resin while still warm. This, how-
 ever, was only done as a final desorption attempt as the
 hot HCl/ H_2O_2 destroys the resin. The overall chemistry
 recovery of the ^{88}Zr was just over ($26 \pm 2\%$) after the
 full chemical processing summarized in the flowsheet in
 Fig. 3. The ^{88}Zr in 2M HCl was concentrated to about
 $100\ \mu\text{L}$ to make the targets.

The low recovery of ^{88}Zr is largely attributed to hydro-
 lysis of the Zr. When the beam initially stops in the
 water cell, the water is approximately pH 5. The ions col-
 lected in the cell were at this pH for 10-20 hours. After
 the irradiation, the water was acidified with HCl to ap-
 proximately pH 1.5, but at this point irreversible species
 seem to have already formed. At pH 5 with dilute Zr
 concentrations ($[\text{Zr}] < 10^{-6}\text{ M}$), the dominant speciation
 for Zr is its hydrolyzed form $\text{Zr}(\text{OH})_4$ [30]. At pH 1.5,
 that species is a more minor constituent with $\text{Zr}(\text{OH})_3^+$
 and $\text{Zr}(\text{OH})_2^{2+}$ dominating. The post-irradiation count-
 ing of the irradiation cell and its window indicated that
 just over one third of the ^{88}Zr produced was sorbed to
 these materials, as opposed to collected in the water sam-
 ples. This is indicative of hydrolysis of the Zr causing it
 to adhere to both the gold and PEEK surfaces.

The precipitation of the Zr has high recovery as it was
 done in a hydroxide precipitate that would carry any
 of the aforementioned Zr species. These species, how-
 ever, behave differently chromatographically from Zr^{4+} ,
 as they cannot form the $\text{Zr}(\text{Cl})_6^{2-}$ anionic complex. Fur-
 ther, the hydrolyzed species are susceptible to adhering
 to surfaces through strong electrostatic interactions that
 inhibit their recovery. This was observed during separa-
 tion chemistry, in which portions of the Zr adhered to
 the polypropylene centrifuge tubes and chromatography
 columns. The bulk of the ^{88}Zr that was not recovered
 during chemistry was lost to the polypropylene centrifuge
 tubes, despite various attempts at desorption.

It is expected that Zr recovery will improve if the beam
 is stopped in more acidic solutions to minimize hydrolysis
 potential or with the addition of strong complexants such
 as fluoride which form stronger complexes than hydroxide.
 The water-filled beam dump at FRIB will operate at
 or near neutral pH, in part due to the logistical challenges
 of executing such an experiment with highly acidic and
 potentially corrosive matrices. Therefore, future studies
 will explore alternative collection methods for hydrolyz-
 able radioactive beam fragments.

The ^{88}Y present in two of the collection bottles was
 isolated prior to recovering the ^{88}Zr . The solutions from
 these two bottles were passed through 50WX8 cation ex-
 change resin (100-200 mesh, $0.8\text{ cm} \times 2\text{ cm}$) that had
 been preconditioned with 0.5M HCl. The resin was rinsed
 with 0.5M HCl, eluting the Zr. During loading and rins-
 ing, the Y was retained on the resin along with most of
 the Sr, while the Zr was collected as an eluate for use
 in the precipitations. The Y was then eluted with 6M
 HCl and concentrated to make the ^{88}Y stock for target

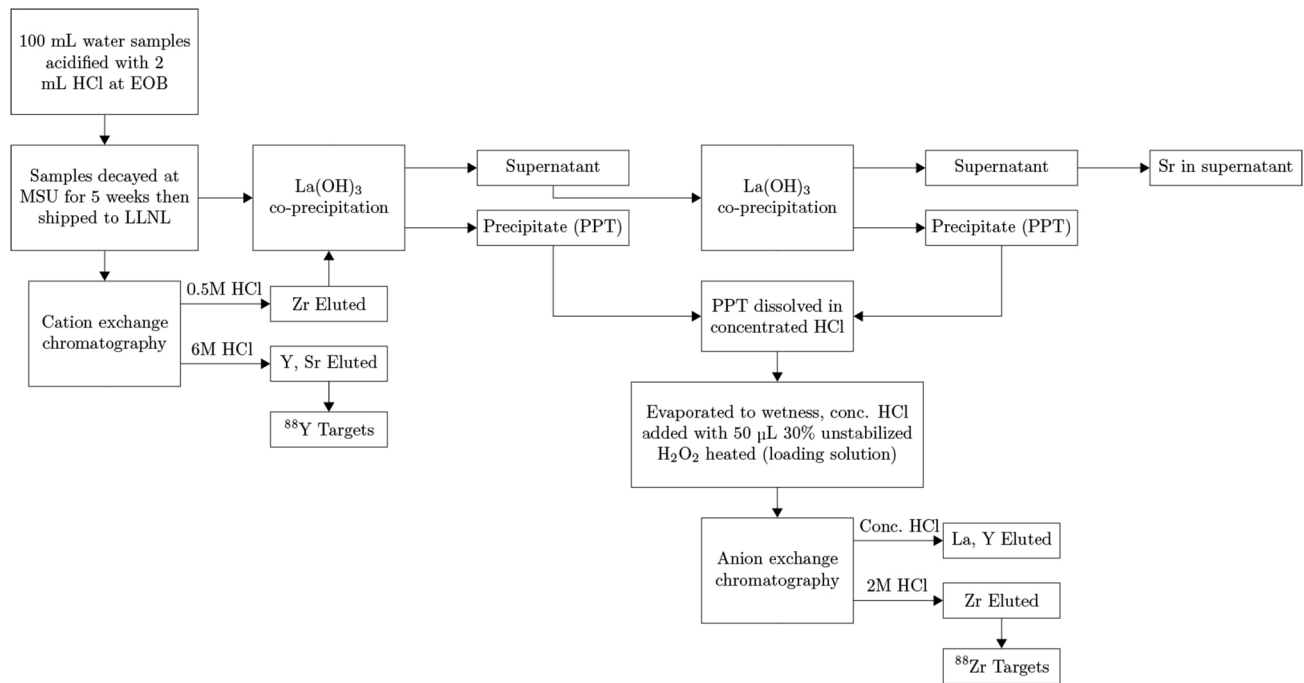


FIG. 3. Flowchart depicting the steps taken to isolate ^{88}Zr and ^{88}Y from the harvested samples for target production.

402 preparation. After separation, 80% of the ^{88}Y was con- 434
 403 centrated as the final Y stock, which had no detectable 435
 404 ^{88}Zr . The Y stock contained 0.9 Ci of ^{88}Y , 0.3 Ci of 436
 405 ^{85}Sr , and 0.02 Ci of ^{83}Rb , which were not further sep- 437
 406 arated because the ^{85}Sr and ^{83}Rb do not interfere with 438
 407 the $^{88}\text{Y}(n,\gamma)^{89}\text{Y}$ measurement. 439

408 Two ^{88}Y and four ^{88}Zr targets were prepared by pipet- 440
 409 ting the respective stocks into 4 mm \times 6 mm (I.D. \times 441
 410 O.D.) Suprasil quartz tubes that had been flame sealed 442
 411 on one end. The Y and Zr in HCl deposits were dried 443
 412 in a water bath evaporator with nitrogen flowed into the 444
 413 tubes. After drying, the tubes were flame sealed and 445
 414 leak-tested. A portion of the ^{88}Y and ^{88}Zr stocks was set 446
 415 aside for characterization. 447

416 The stable element content in the samples was deter- 448
 417 mined with inductively coupled plasma-mass spectrometry 449
 418 (ICP-MS) by analyzing aliquots consisting of 100 μL 450
 419 of the ^{88}Y and ^{88}Zr stocks that had been diluted to 5 mL 451
 420 with 2% HNO_3 . In the ^{88}Zr targets, the stable Sr, Y, Zr, 452
 421 Nb, Mo, and La content was found to be in the range 453
 422 0.79-2.3 ng, 0.03-0.07 ng, 27-79 ng, 0.4-1.1 ng, 6.2-18 ng, 454
 423 and 0.03-0.09 ng for each metal, respectively. In the ^{88}Y 455
 424 targets, the stable Sr, Y, Zr, Nb, Mo, and La content 456
 425 was found to be in the range 15-25 ng, 0.94-1.6 ng, 5.5-
 426 9.0 ng, 0.02-0.03 ng, 1.4-2.4 ng, and 18-29 ng for each
 427 metal, respectively. Despite the La carrier initially being 457
 428 present at nearly 10^9 times the ^{88}Zr mass (7.4×10^{-12} g) 458
 429 after co-precipitation, it was successfully separated with
 430 a decontamination factor of 10^8 . The stable element con- 459
 431 tent in each sample was low enough that it did not inter- 460
 432 fere with the subsequent cross-section measurements. 461
 433 For stable Zr content, this was demonstrated with the 462

Zr monitors. For the 60 mg Zr monitor, ^{89}Zr activity 434
 435 produced via the $^{90}\text{Zr}(n,2n)^{89}\text{Zr}$ reaction was less than
 436 10% of that observed in the co-irradiated ^{88}Zr samples.
 437 With 10^{-6} times less stable Zr present in the ^{88}Zr sam-
 438 ple, the percent contribution of ^{89}Zr from this source is
 439 negligible. Here the stable Zr content did not impact
 440 the subsequent cross-section measurements, however this
 441 will have to be assessed on a reaction-by-reaction basis
 442 for future measurements.

The sealed samples were characterized with γ -ray spec- 443
 444 troscopy to assess the initial amounts of each radionu-
 445 clide. The γ -ray spectrum of a typical ^{88}Zr target is
 446 shown in Fig. 4a. Although the yield of the chemistry
 447 was only 26%, the radiopurity of the ^{88}Zr sample was
 448 high - the only other radionuclide present in the ^{88}Zr
 449 targets was its decay daughter, ^{88}Y , which grew in after
 450 the ^{88}Zr separation. At the end of separation, the atom
 451 ratio of ^{88}Zr to ^{88}Y was on the order of 10^3 . A typical γ -
 452 ray spectrum from a ^{88}Y target is shown in Fig. 4c. The
 453 dominant species are ^{88}Y and ^{85}Sr . Other minor features
 454 in the spectrum are escape peaks from the 1836.063-keV
 455 γ ray from the decay of ^{88}Y , the 511-keV annihilation
 456 peak, and the photopeaks due to the decay of ^{83}Rb .

IV. NEUTRON-CAPTURE CROSS-SECTION MEASUREMENTS

The cross sections were determined through the acti-
 vation method using γ -ray spectroscopy to measure the
 burnup of the target and, in the case of ^{88}Zr , the pro-
 duction of the capture product after neutron irradiation.

TABLE II. Summary of characteristics for each target used for subsequent neutron irradiation

Target No.	Radionuclide	Activity at beginning of irradiation (kBq)	Irradiation Time (h)	Irradiation Facility	Cadmium Covered
1	^{88}Zr	3.31 ± 0.11	1	MURR	No
2	^{88}Zr	3.63 ± 0.12	10	MURR	No
3	^{88}Zr	3.81 ± 0.12	12	MNRC	No
4	^{88}Zr	4.68 ± 0.19	12	MNRC	Yes
5	^{88}Y	7.17 ± 0.30	1	MURR	No
6	^{88}Y	4.34 ± 0.18	10	MURR	No

The samples were shipped to MURR and MNRC for irradiation.

At MURR, one set of samples was irradiated for 1 hour and a second one for 10 hours in the graphite reflector. Each set contained a ^{88}Zr sample, a ^{88}Y sample, and a collection of monitor foils individually encapsulated in quartz. The monitor foils for the 1-hour irradiation contained stable Zr, Fe, and Mo while the 10-hour set contained only Zr and Fe; Mo was not included in this set because of the high level of activity that would be produced.

After irradiation, the samples were removed from the reactor, extracted from the irradiation canister in a hot cell, and packaged for shipping. The samples were shipped back to LLNL and the exteriors cleaned with aqua regia and 18.2 M Ω ·cm water washes to remove any contamination. The samples were then opened and the residues dissolved with 9 M HCl (~ 500 μL), which were diluted with 18.2 M Ω ·cm water to 10 mL. Starting 3 days after the irradiation, these ^{88}Y and ^{88}Zr samples were counted for approximately 1 month to track the decay of the γ -ray lines shown in Figs. 4b and 4d. The population of ^{88}Zr , ^{89}Zr , and ^{88}Y atoms were determined from the intensity of the characteristic γ -ray peaks detected at 909.15 keV, 392.87 keV, and 898.042 keV, respectively [29, 31]. The monitor foils were extracted from the quartz vial and individually counted to quantify the dominant activation products from the γ -ray peaks at energies listed in parentheses: ^{59}Fe (1099.245 and 1291.59 keV), ^{95}Zr (724.192 and 756.725 keV), ^{97}Zr (743.36 keV), and ^{99}Mo (181.068 and 739.5 keV).

At MNRC, two sets of samples containing ^{88}Zr and Fe, Zr, and Mo monitor foils separately encapsulated in quartz were irradiated for 12 hours in the Neutron Transmutation Doping (NTD) location. This location has the highest ratio of thermal (< 0.5 eV) to fast (> 1 MeV) neutrons in the MNRC reactor, with thermal and resonance region flux values determined from the monitor foils shown in Table III. The neutron flux in that location was modeled using MCNP5 (Fig. 5) to demonstrate the shape of the epithermal neutron region. The non-lethargy-normalized flux values obtained from MCNP5 were fit with the equation:

$$\Phi_{ep}(E) = \Phi_{ep,c} \frac{(1\text{eV})^\alpha}{E^{1+\alpha}} \quad (1)$$

where $\Phi_{ep,c}$ is a proportionality constant to determine the epithermal neutron shape factor, α [32]. For an ideal 1/E spectrum, α is 0 while we calculated a value for α of 0.35. It should be noted that this epithermal neutron shape factor determined from the model only describes the general shape of the spectrum averaging out local features unique to the irradiation position.

One set of samples was irradiated with a 1-mm-thick cadmium wrapping, to reduce the thermal flux by about two orders of magnitude. After irradiation, the samples remained at MNRC for 2.5 days to allow the shortest-lived activities to decay away. They were then returned to LLNL where the exteriors were wiped clean and counted within 3 days following the irradiation. The monitor foils were counted in the same manner as the MURR samples. Typical γ -ray spectra of the samples before and after irradiation are shown in Fig. 6.

A. Thermal and resonance-region cross sections for ^{88}Zr

The ^{88}Zr and ^{89}Zr atom populations were quantified using their characteristic γ rays at 392.87 keV and 909.15 keV ($I_\gamma = 99.04\%$), respectively [29, 31]. The 909-keV peak in the MURR-irradiated samples was found to decay with an average half-life of 3.27 ± 0.02 days, which agrees with the well-established value of 3.267 ± 0.005 d for the half-life of ^{89}Zr . The less intense transitions at 1657, 1713, and 1745 keV from the decay of ^{89}Zr were also observed. The 909-keV peak is clearly the result of ^{89}Zr decay based on the half-life and presence of multiple γ -ray lines.

The inferred number of ^{88}Zr and ^{89}Zr atoms was corrected for decay both during and after irradiation. While the decay during irradiation for ^{88}Zr is less than a 2% effect, the correction for ^{89}Zr is up to 6% for the 10-hour MURR irradiations. The measured ground state ^{89}Zr atoms originate from the decay of ^{89m}Zr , which is predominantly populated in the radiative-capture process due to angular-momentum considerations. The deduced number of ^{89}Zr atoms therefore has to be adjusted for the branching ratio of ^{89m}Zr , which decays by isomeric transition to the ground state 93.77% of the time [31]. The resulting ^{89}Zr population was then normalized to the initial ^{88}Zr population to adjust for differences in ^{88}Zr in

TABLE III. Measured thermal and resonance region neutron flux from MURR and MNRC determined from the Fe, Zr, and Mo flux monitors irradiated alongside the ^{88}Zr and ^{88}Y samples. The average flux was determined from 3 or 4 neutron-capture reactions with known cross sections depending on whether a Mo foil was included.

Sample	Irradiation Time (h)	Measured Average Flux ($\text{n}/\text{cm}^2\text{s}$)		Thermal/Resonance	Monitor Foils
		Thermal	Resonance		
MURR	1.0	$(7.71 \pm 0.46) \times 10^{13}$	$(2.33 \pm 0.22) \times 10^{12}$	33	Fe, Zr, Mo
MURR	10.2	$(8.05 \pm 0.50) \times 10^{13}$	$(2.30 \pm 0.22) \times 10^{12}$	35	Fe, Zr
MNRC	12.0	$(2.54 \pm 0.15) \times 10^{11}$	$(3.94 \pm 0.36) \times 10^9$	65	Fe, Zr, Mo
MNRC/Cd-lined	12.0	$(1.55 \pm 0.17) \times 10^9$	$(2.86 \pm 0.26) \times 10^9$	0.54	Fe, Zr, Mo

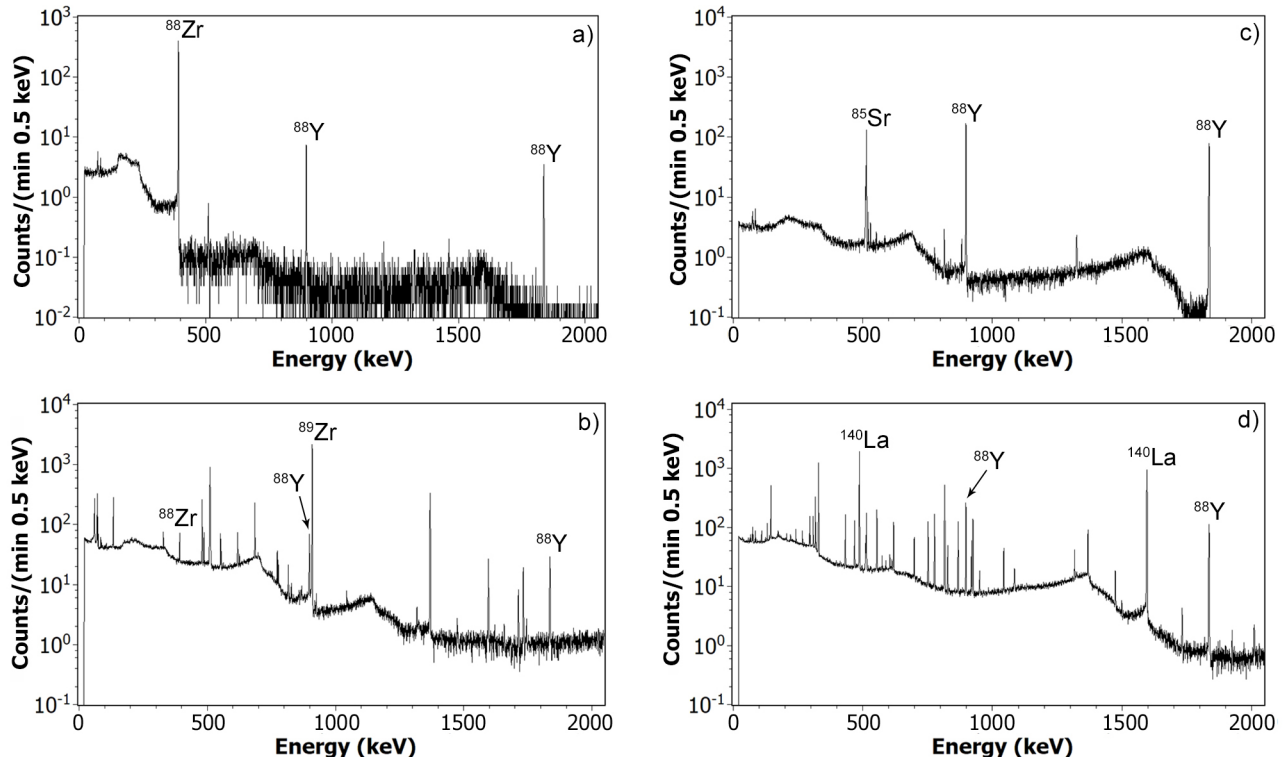


FIG. 4. γ -ray spectra of a) ^{88}Zr target before irradiation, b) ^{88}Zr target after 10-hour irradiation at MURR and 3.6 d decay, c) ^{88}Y target before irradiation, and d) ^{88}Y target after 10-hour irradiation at MURR and 7.4 d decay. Decay and efficiency corrections have not been applied. The initial ^{88}Zr activity was accompanied by ^{88}Y , which grew in from the decay following chemical separation. After irradiation, the ^{88}Zr activity was greatly reduced and a large quantity of ^{89}Zr was present. Conversely, no ^{88}Y burnup was observed in the ^{88}Y targets after irradiation. The initial ^{88}Y activity was accompanied by ^{85}Sr and a small amount of ^{83}Rb . After irradiation, ^{140}La , the radiative capture product on stable ^{139}La , was also observed.

550 each target. The thermal-neutron-capture cross section 562
 551 for ^{89}Zr was previously constrained to 1.2×10^4 b [25], 563
 552 which has been supported with recent nuclear data calcu- 564
 553 lations [33]. Despite the large magnitude of the predicted 565
 554 and constrained cross section for ^{89}Zr , it is still 1.5% that 566
 555 of ^{88}Zr , and thus the subsequent burnup of ^{89}Zr via ra- 567
 556 diative capture is a negligible loss mechanism within the 568
 557 uncertainty of this measurement.

558 The MNRC irradiation provided measurements with 571
 559 two different neutron-energy spectra, obtained with and 572
 560 without the thermal-neutron flux suppressed by a Cd 573
 561 absorber. From the results of these two irradiations,

the thermal-neutron-capture cross section and resonance
 integral from ^{88}Zr were determined using methods de-
 scribed in Refs. [34–36]. The thermal and resonance-
 region neutron-flux values (Φ_T and Φ_{ep} , respectively)
 were determined from the monitor-foil reactions which
 have well known neutron-capture cross sections in these
 two energy regions [37]. The average neutron flux the
 samples were exposed to is presented in Table III. The
 unlined sample was exposed to a thermal-neutron flux
 over two orders of magnitude larger than the Cd-lined
 sample. The initial number of ^{88}Zr atoms ($N_{88}(0)$) in
 the unlined and Cd-lined samples and the atoms of ^{89}Zr

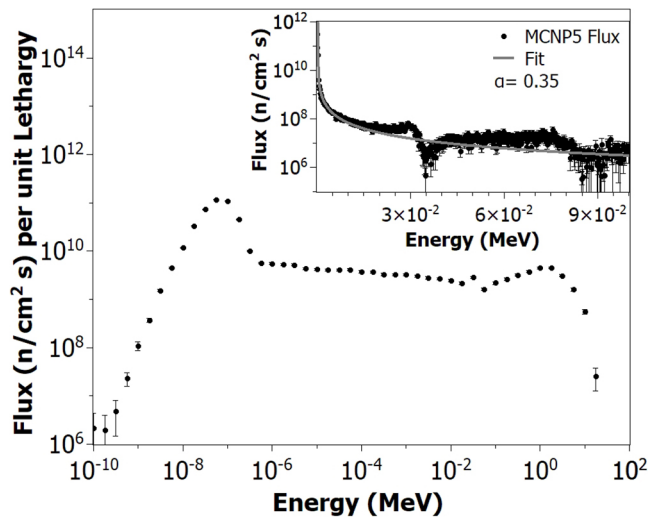


FIG. 5. Neutron energy spectra of MNRC reactor in NTD void location calculated using MCNP5. The main figure displays the full energy range on log-scale with lethargy-normalized flux. The inset features a more detailed model of the epithermal region on a linear energy scale with the non-normalized flux. More points were used to model this region to allow for a fit (gray solid line) to determine the epithermal-neutron shape factor. Both calculations include the 1-cm thick Al sample holder.

574 present after irradiation (N_{89}) were determined in the
575 same way as with the MURR samples.

576 The cross sections for the thermal (σ_T) and resonance
577 region (I) were extracted using the equation:

$$N_{89}(\Phi) = N_{88}(0) \left[1 - e^{-t_i(\sigma_T \Phi_T + I \Phi_{ep})} \right] \quad (2)$$

578 where t_i is the irradiation time, which was the same
579 for both irradiations. As the energies and widths of the
580 ^{88}Zr resonances have not yet been measured, the reported
581 value for I is uncorrected for $1/v$ behavior, as this cannot
582 be assumed from the existing measurements.

583 Based on these measurements, the thermal-neutron-
584 capture cross section and uncorrected resonance integral
585 for $^{88}\text{Zr}(n,\gamma)^{89}\text{Zr}$ were determined to be $(8.81 \pm 0.63) \times$
586 10^5 b and $(2.53 \pm 0.28) \times 10^6$ b, respectively. While the
587 resonance integral here was found to be a factor 3 greater
588 than the thermal cross section, this ratio is in line with
589 other I/σ ratios, especially for other isotopes near ^{88}Zr
590 [37, 38]. To the best of our knowledge, this resonance
591 integral is the largest measured to date by a factor of 601
592 100 over the second largest, ^{155}Eu ($I=2.32 \times 10^4$ b) [39]. 602
593 Given the magnitude of the cross sections here and poten- 603
594 tial for unexpected behavior as a result of this, a further 604
595 evaluation of resonance widths and locations is required 605
596 to give a more complete picture of the resonance inte- 606
597 gral. The 1σ uncertainties here for the thermal-neutron- 608
598 capture cross section and resonance integral are about 609
599 7% and 11%, respectively. The uncertainties in the re- 610
600 sults were driven by correlated contributions from the 611

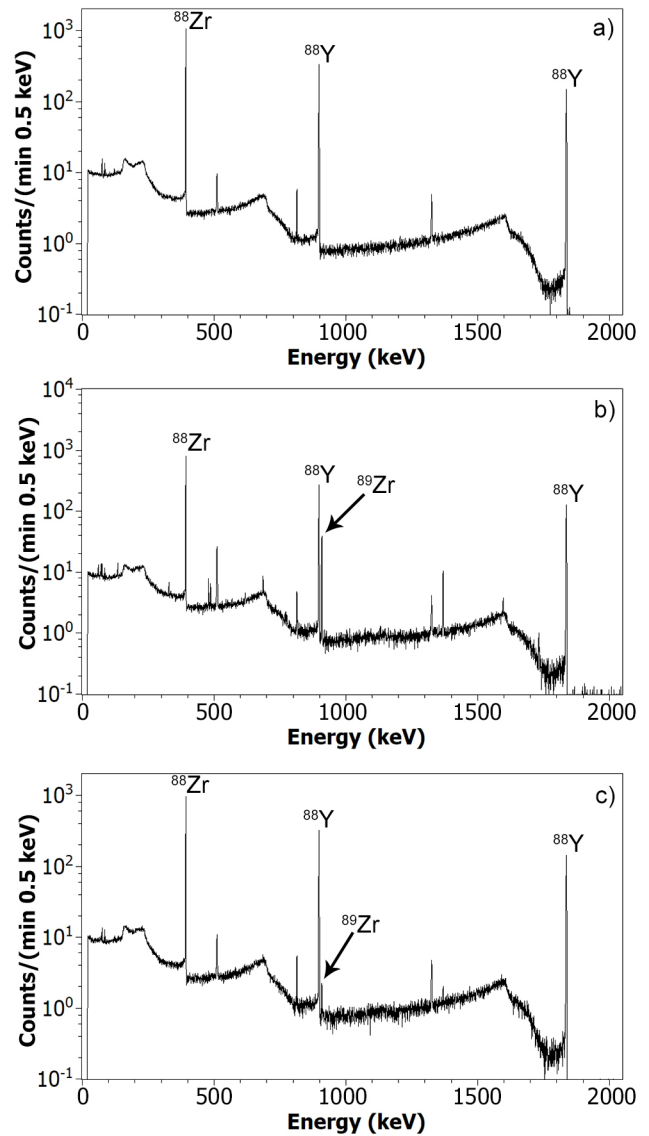


FIG. 6. Typical γ -ray spectra of a ^{88}Zr target a) before irradiation, b) after irradiation at MNRC, and c) after irradiation at MNRC in a Cd-lined container. Decay and efficiency corrections have not been applied. The initial target contained only ^{88}Zr and its daughter ^{88}Y and after irradiation a decrease in the ^{88}Zr and an increase in the ^{89}Zr were observed. When the thermal-neutron flux was suppressed with the Cd-liner, the ^{88}Zr burnup and ^{89}Zr production were both reduced.

nuclear data of known cross sections for the monitor foil reactions used to determine the neutron flux. The main uncorrelated contribution was from the counting geometry uncertainty. Other minor uncertainty contributions arise from nuclear counting statistics, masses, irradiation times, and photopeak efficiencies. For the two samples sent to MURR, the thermal-neutron-capture cross section for ^{88}Zr (σ_T) was calculated from the production of ^{89}Zr using Eq. 2. The value for the resonance integral, I , determined from the MNRC measurement was used

TABLE IV. Summary of 1σ uncertainty contributions for each aspect of the experiment. The final uncertainty on each measurement was assessed by weighting the listed contributions and assessing their impact on the central value. Correlated uncertainties were common across each measurement listed in Table II, while uncorrelated uncertainties varied from sample-to-sample.

Source of Uncertainty	Magnitude	Correlated/Uncorrelated
Chemical composition and yield		
Counting statistics	< 3 %	Uncorrelated
Sample geometry	3 %	Uncorrelated
Point-source calibration of HPGe efficiency	1 %	Correlated
Dilutions by mass	< 0.5 %	Uncorrelated
Mass spectrometry	0.5 – 10 %	Uncorrelated
Neutron Flux		
Monitor mass	0.3 – 7.4 %	Uncorrelated
Irradiation time	< 0.8 %	Uncorrelated
Sample geometry	3 %	Uncorrelated
Point-source calibration of HPGe efficiency	1 %	Correlated
Counting statistics	< 2 %	Uncorrelated
Reference cross-section data, thermal	5.6 %	Correlated
Reference cross-section data, resonance	8.8 %	Correlated
Final-to-initial atom ratios		
Sample geometry	6 %	Uncorrelated
Point-source calibration of HPGe efficiency	1 %	Correlated
Counting statistics	0.5 – 4.6 %	Uncorrelated

here. The thermal and resonance region neutron capture cross sections on ^{89}Zr were previously determined to be small relative to the ^{88}Zr values [24], and thus are neglected. The thermal-neutron-capture cross sections for $^{88}\text{Zr}(n,\gamma)^{89}\text{Zr}$ calculated from ^{89}Zr production for the 1 hour and 10 hour irradiations at MURR are $(8.55\pm 0.63) \times 10^5$ b and $(7.78\pm 0.59) \times 10^5$ b, respectively.

The thermal-neutron-capture cross section for ^{88}Zr was also determined from the disappearance of ^{88}Zr using

$$N_{88}(\Phi) = N_{88}(0)e^{-t_i(\sigma_T\Phi_T + I\Phi_{ep})} \quad (3)$$

which is effectively the complement of Eq. 2. From the burnup of ^{88}Zr , the thermal-neutron-capture cross-sections for $^{88}\text{Zr}(n,\gamma)^{89}\text{Zr}$ were found to be $(8.40\pm 0.63) \times 10^5$ b and $(6.99\pm 0.55) \times 10^5$ b for the 1 hour and 10 hour irradiations, respectively. The average of the four thermal-neutron-capture cross-sections measured at MURR and the one measured at MNRC is $(8.04\pm 0.63) \times 10^5$ b, where the uncertainties between the measurements are highly correlated and therefore are not reduced. The thermal-neutron-capture cross section can be compared with the previously measured value of $(8.61\pm 0.69) \times 10^5$ b [25]. However, the analysis of the present work separately takes into account the contribution of the resonance integral and the thermal-neutron contribution whereas the previous result attributed all reactions to the thermal flux. The impact of including the resonance integral in an analogous way for the previous result reduces the thermal cross section by about 10%. Good agreement is obtained between the two sets of measurements.

B. Thermal neutron capture cross section ^{88}Y

The neutron-capture cross section for ^{88}Y is more difficult to determine because the reaction product, ^{89}Y , is stable. Therefore, with decay spectroscopy, the only available signature was a decrease in ^{88}Y activity following irradiation that exceeded that expected from radioactive decay. For the ^{88}Y samples, the characteristic γ -ray peaks at 898 and 1836 keV were prominent both before and after neutron irradiation. After accounting for decay losses, the number of ^{88}Y atoms remained constant within uncertainty following both the 1 and 10 hour irradiations at MURR. As such, a limit could be set for the cross section using Eq. 3 together with the estimate that the minimum detectable ^{88}Y burnup $(\frac{N_{88}(\Phi)}{N_{88}(0)})$ in the experiment is the 2σ uncertainty limited by the 3% geometric counting uncertainty. For this calculation, the resonance region contribution was not considered. Based on the data collected for the sample irradiated for 10 hours, an upper limit of 1.8×10^4 b was obtained for the thermal-neutron-capture cross section on ^{88}Y . This value is therefore at least 400 times smaller than that of ^{88}Zr , and further supports that the large ^{88}Zr neutron-capture cross section is not associated with the nearby $N=50$ neutron-shell closure [24], as ^{88}Y is only one neutron away while ^{88}Zr is two neutrons away. The predicted neutron-capture cross section for ^{88}Y is 18.7 b [33], which falls well within the limit established here.

V. CONCLUSION

Aqueous harvesting was used to collect and purify ^{88}Zr from a mixture of ^{92}Mo fragmentation products that had been stopped in a water cell at the NSCL. The chemical recovery efficiency achieved for ^{88}Zr was $(26\pm 2)\%$; however, the radiopurity was nearly 100% following chemical separation, with the only radioactive contaminant being the subsequent ingrowth of the ^{88}Y daughter. Previous experiments achieved greater recovery efficiencies for secondary beams of ^{22}Na [12] and ^{67}Cu [13, 14], but challenges were encountered for ^{48}V [15] that were similar to what was encountered during this ^{88}Zr harvesting experiment. This set of experiments, although limited, seems to indicate that species that are readily hydrolyzed will be more difficult to efficiently collect via aqueous harvesting at FRIB in a water beam dump.

The accumulation of ^{88}Zr in a single aqueous sample lasted for up to 16 hours, giving ample time for even kinetically-slow chemical processes to occur. Circulating the water in the FRIB beam dump directly into a chemistry setup [40] to minimize the time between irradiation and chemistry will likely help minimize the surface adsorption, especially for the kinetically-slower processes. Recently, a hollow fiber supported liquid membrane (HF-SLM) coated with the extractant Aliquat 336 was used to extract ^{48}V . This method was intended to simulate a circulating aqueous harvesting experiment and demonstrated an extraction efficiency of 71% for ^{48}V present at the part-per-trillion level in an aqueous matrix [41]. The addition of complexants or acids that interact with these metals to the circulating water may also allow for higher recovery efficiency.

Using an energetic charged-particle beam to produce $^{88,89}\text{Zr}$ from ^{89}Y in solution could induce a similar water radiolysis condition that may be aiding in the Zr hydrolysis and will also allow for shorter irradiations and kinetic studies [42, 43]. Given that the group IV and V metals tend to hydrolyze above pH 1.5, future efforts targeting these species should focus on alternative harvesting methodologies, such as circulating aqueous systems, use of complexants, or transitioning to other phases of har-

vesting, such as implementation of solid collectors.

The results obtained from the MURR and MNRC irradiations of samples produced from the isotopes collected at the NSCL yielded a weighted average thermal-neutron-capture cross-section for ^{88}Zr of $(8.04\pm 0.63) \times 10^5$ b and an uncorrected resonance integral of $(2.53\pm 0.28) \times 10^6$ b. In addition, an upper limit on the thermal neutron $^{88}\text{Y}(n,\gamma)^{89}\text{Y}$ cross section was established to be 1.8×10^4 b.

Despite the chemistry challenges, this work was the first demonstration of the sequence of steps needed to collect radioisotopes deposited in an aqueous target at a fragmentation facility and to use that material for subsequent cross-section measurements. The production rates of ^{88}Zr at FRIB are expected to reach approximately 3×10^4 times higher than at the NSCL and would yield about 630 mCi of ^{88}Zr per week. Additionally, new instruments such as the Device for Indirect Neutron Capture Experiments on Radionuclides (DICER) at the Los Alamos Neutron Science Center (LANSCE) could be used for detailed investigations of the resonance region neutron-capture cross sections [44]. With the higher production rates at FRIB and access to new tools to study neutron capture reactions, additional cross-section measurements relevant to stockpile stewardship and nuclear astrophysics could be pursued.

ACKNOWLEDGMENTS

We acknowledge the staff of the NSCL, particularly the operation and A1900 staff for experiment coordination and providing beam. We thank J. Yurkon for Au-sputtering of the Ti window. We thank P. T. Woody for nuclear counting support and R. Lindvall for the ICPMS analysis. We also thank the operators and radiation safety staff at MURR and MNRC for experimental support at the reactors. At LLNL, this work was funded through LDRD 16-ERD-022 and was performed under the auspices of the US Department of Energy under contract DE-AC52-07NA27344. SRM and GFP were supported under DESC0013662. SEL and CSL were supported US Department of Energy under grant DESC-0015558.

-
- [1] E. P. Abel, M. Avilov, V. Ayres, E. Birnbaum, G. Bollen, G. Bonito, T. Bredeweg, H. Clause, A. Couture, J. Devore, M. Dietrich, P. Ellison, J. Engle, R. Ferreri, J. Fitzsimmons, M. Friedman, D. Georgobiani, S. Graves, J. Greene, S. Lapi, C. S. Loveless, T. Mastren, C. Martinez-Gomez, S. McGuinness, W. Mittig, D. Morrissey, G. Peaslee, F. Pellemoine, J. D. Robertson, N. Scielzo, M. Scott, G. Severin, D. Shaughnessy, J. Shusterman, J. Singh, M. Stoyer, L. Sutherlin, A. Visser, and J. Wilkinson, Isotope harvesting at FRIB: additional opportunities for scientific discovery, *Journal of Physics G: Nuclear and Particle Physics* **46**, 100501 (2019).

- [2] D. Schumann, J. Neuhausen, I. Dillmann, C. Domingo Pardo, F. Käppeler, J. Marganec, F. Voss, S. Walter, M. Heil, R. Reifarh, J. Goerres, E. Uberseder, M. Wiescher, and M. Pignatari, Preparation of a ^{60}Fe target for nuclear astrophysics experiments, *Nuclear Instruments and Methods in Physics Research, Section A* **613**, 347 (2010).
- [3] G. Rugel, T. Faestermann, K. Knie, G. Korschinek, M. Poutivtsev, D. Schumann, N. Kivel, I. Günther-Leopold, R. Weinreich, and M. Wohlmuther, New mea-

- 771 surement of the Fe60 half-life, Physical Review Letters 835
 772 **103**, 072502 (2009). 836
- 773 [4] A. Wallner, M. Bichler, K. Buczak, R. Dressler, L. K. 837
 774 Fifield, D. Schumann, J. H. Sterba, S. G. Tims, G. Wall- 838
 775 ner, and W. Kutschera, Settling the half-life of Fe 60: 839
 776 Fundamental for a versatile astrophysical chronometer, 840
 777 Physical Review Letters **114**, 041101 (2015). 841
- 778 [5] K. M. Ostdiek, T. S. Anderson, W. K. Bauder, M. R. 842
 779 Bowers, A. M. Clark, P. Collon, W. Lu, A. D. Nelson, 843
 780 D. Robertson, M. Skulski, R. Dressler, D. Schumann, 844
 781 J. P. Greene, W. Kutschera, and M. Paul, Activity mea- 845
 782 surement of Fe 60 through the decay of Co 60m and con- 846
 783 firmation of its half-life, Physical Review C **95**, 055809 847
 784 (2017), arXiv:1612.00006. 848
- 785 [6] E. Uberseder, R. Reifarh, D. Schumann, I. Dillmann, 849
 786 C. Domingo Pardo, J. Gorres, M. Heil, F. Kappeler, 850
 787 J. Marganec, J. Neuhausen, M. Pignatari, F. Voss, 851
 788 S. Walter, and M. Wiescher, Measurement of the 852
 789 $60\text{Fe}(n,\gamma)61\text{Fe}$ cross section at stellar temperatures, 853
 790 Physical Review Letters **102**, 151101 (2009). 854
- 791 [7] T. Heftrich, M. Bichler, R. Dressler, K. Eberhardt, 855
 792 A. Endres, J. Glorius, K. Göbel, G. Hampel, M. Heftrich, 856
 793 F. Käppeler, C. Lederer, M. Mikorski, R. Plag, 857
 794 R. Reifarh, C. Stieghorst, S. Schmidt, D. Schumann, 858
 795 Z. Slavkovská, K. Sonnabend, A. Wallner, M. Weigand, 859
 796 N. Wiehl, and S. Zauner, Thermal neutron capture cross 860
 797 section of the radioactive isotope Fe 60, Physical Review 861
 798 C **92**, 015806 (2015), arXiv:arXiv:1507.03152v1. 862
- 799 [8] D. Schumann, N. Kivel, and R. Dressler, Production and 863
 800 characterization of 60Fe standards for accelerator mass 864
 801 spectrometry, PLoS ONE **14**, 4 (2019). 865
- 802 [9] M. Ayrarov and D. Schumann, Preparation of 26Al , 866
 803 59Ni , 44Ti , 53Mn and 60Fe from a proton irradiated cop- 867
 804 per beam dump, Journal of Radioanalytical and Nuclear 868
 805 Chemistry **286**, 649 (2010). 869
- 806 [10] S. Heinitz, D. Kiselev, N. Kivel, and D. Schumann, Sepa- 870
 807 ration of weighable amounts of 10Be from proton irradiated 871
 808 graphite, Applied Radiation and Isotopes **130**, 260 872
 809 (2017). 873
- 810 [11] B. D. Schumann, T. Stowasser, R. Dressler, and M. Ayrarov, 874
 811 Possibilities of preparation of exotic radionuclide 875
 812 samples at PSI for scientific investigations, Radiochimica 876
 813 Acta **101**, 501 (2013). 877
- 814 [12] A. Pen, T. Mastren, G. F. Peaslee, K. Petrasky, P. A. 878
 815 Deyoung, D. J. Morrissey, and S. E. Lapi, Design and 879
 816 construction of a water target system for harvesting radioisotopes 880
 817 at the National Superconducting Cyclotron Laboratory, Nuclear Instruments and Methods in Physics 881
 818 Research, Section A: Accelerators, Spectrometers, Detectors and Associated Equipment **747**, 62 (2014). 882
- 819 [13] T. Mastren, A. Pen, G. F. Peaslee, N. Wozniak, S. Loveless, 883
 820 S. Essenmacher, L. G. Sobotka, D. J. Morrissey, and 884
 821 S. E. Lapi, Feasibility of isotope harvesting at a projectile fragmentation facility: 67Cu , Scientific Reports **4**, 1 885
 822 (2014). 886
 823 887
 824 888
- 825 [14] T. Mastren, A. Pen, S. Loveless, B. V. Marquez, 889
 826 E. Bollinger, B. Marois, N. Hubley, K. Brown, D. J. Morrissey, 890
 827 G. F. Peaslee, and S. E. Lapi, Harvesting 67Cu 891
 828 from the Collection of a Secondary Beam Cocktail at the 892
 829 National Superconducting Cyclotron Laboratory, Analytical Chemistry **87**, 10323 (2015). 893
 830 894
 831 895
- 832 [15] C. S. Loveless, B. E. Marois, S. J. Ferran, J. T. Wilkinson, 896
 833 L. Sutherlin, G. Severin, J. A. Shusterman, N. D. 897
 834 Scielzo, M. A. Stoyer, D. J. Morrissey, J. D. Robertson, 898
- G. F. Peaslee, and S. E. Lapi, Harvesting 48V at the National Superconducting Cyclotron Laboratory, Applied Radiation and Isotopes **157**, 1 (2020).
- [16] E. P. Abel, H. K. Clause, and G. W. Severin, Radiolysis and radionuclide production in a flowing-water target during fast $40\text{Ca}(20+)$ irradiation., Applied Radiation and Isotopes **158**, 1 (2020).
- [17] T. Kobayashi, T. Sasaki, I. Takagi, and H. Moriyama, Solubility of Zirconium (IV) Hydrrous Oxides, Journal of Nuclear Science and Technology **44**, 90 (2007).
- [18] M. A. Deri, B. M. Zeglis, L. C. Francesconi, and J. S. Lewis, PET Imaging with 89Zr : From Radiochemistry to the Clinic, Nucl. Med. Biol. **40**, 3 (2013).
- [19] A. Baimukhanova, V. Radchenko, J. Kozempel, A. Marinova, V. Brown, V. Karandashev, D. Karaivanov, P. Schaffer, and D. Filosofov, Utilization of (p, n) reaction for 86Zr production with medium energy protons and development of a $86\text{Zr} \rightarrow 86\text{Y}$ radionuclide generator, Journal of Radioanalytical and Nuclear Chemistry **316**, 191 (2018).
- [20] K. Sonnabend, P. Mohr, A. Zilges, R. Hertenberger, H.-F. Wirth, G. Graw, and T. Faestermann, First excited state of the s-process branching nucleus 95Zr , Physical Review C **68**, 048802 (2003).
- [21] R. D. Hoffman, K. Kelley, F. S. Dietrich, R. Bauer, and M. Mustafa, UCRL-TR-222275, Tech. Rep. (Lawrence Livermore National Laboratory, Livermore, CA, 2006).
- [22] A. C. Larsen, M. Guttormsen, R. Schwengner, D. L. Bleuel, S. Goriely, S. Harissopulos, F. L. Bello Garrote, Y. Byun, T. K. Eriksen, F. Giacoppo, A. Görgen, T. W. Hagen, M. Klintefjord, T. Renstrøm, S. J. Rose, E. Sahin, S. Siem, T. G. Tornyi, G. M. Tveten, A. V. Voinov, and M. Wiedeking, Experimentally constrained $(p,\gamma)89\text{Y}$ and $(n,\gamma)89\text{Y}$ reaction rates relevant to p-process nucleosynthesis, Physical Review C **93**, 045810 (2016), arXiv:arXiv:1510.00969v2.
- [23] V. Reis, R. Hanrahan, and K. Levedahl, The Big Science of stockpile stewardship, Physics Today , 46 (2016).
- [24] R. J. Prestwood, K. W. Thomas, D. R. Nethaway, and N. L. Smith, Measurement of 14-MeV Neutron Cross Sections for 88Zr and 88Y , Physical Review C **29**, 805 (1984).
- [25] J. A. Shusterman, N. D. Scielzo, K. J. Thomas, E. B. Norman, S. E. Lapi, C. S. Loveless, N. J. Peters, J. D. Robertson, D. A. Shaughnessy, and A. P. Tonchev, The surprisingly large neutron capture cross-section of Zr-88 , Nature **565**, 328 (2019).
- [26] P. L. Brown, E. Curti, B. Grambow, and C. Ekberg, Chemical Thermodynamics of Zirconium, vol. 8 ed., edited by F. J. Mompean, J. Perrone, and M. Illemassene (OECD Nuclear Energy Agency, 2005).
- [27] A. Stolz, T. Baumann, T. Ginter, D. Morrissey, M. Portillo, B. Sherrill, M. Steiner, and J. Stetson, Production of rare isotope beams with the NSCL fragment separator, Nuclear Instruments & Methods in Physics Research B **241**, 858 (2005).
- [28] D. J. Morrissey, B. M. Sherrill, M. Steiner, A. Stolz, and I. Wiedenhoever, Commissioning the A1900 projectile fragment separator, Nuclear Instruments & Methods in Physics Research B **204**, 90 (2003).
- [29] E. A. McCutchan and A. A. Sonzogni, Nuclear Data Sheets for $A = 88$, Nuclear Data Sheets **115**, 135 (2014).
- [30] C. Ekberg, G. Källvenius, Y. Albinsson, and P. L. Brown, Studies on the hydrolytic behavior of zirconium(IV),

- Journal of Solution Chemistry **33**, 47 (2004). 928
- [31] B. Singh, Nuclear Data Sheets for $A = 89$, Nuclear Data 929
Sheets **114**, 1 (2013). 930
- [32] H. Yücel and M. Karadag, Experimental determination 931
of the α -shape factor in the $1/E$ $1+\alpha$ epithermal-isotopic 932
neutron source-spectrum by dual monitor method, An- 933
nals of Nuclear Energy **31**, 681 (2004). 934
- [33] A. Koning, D. Rochman, J. C. Sublet, N. Dzysiuk, 935
M. Fleming, and S. van der Marck, TENDL: Complete 936
Nuclear Data Library for Innovative Nuclear Science and 937
Technology, Nuclear Data Sheets **155**, 1 (2019). 938
- [34] H. Harada, S. Nakamura, T. Katoh, and Y. Ogata, Mea- 939
surement of Thermal Neutron Cross Section and Reso- 940
nance Integral of the Reaction $99\text{Tc}(n, \gamma)100\text{Tc}$, Journal 941
of Nuclear Science and Technology **32**, 395 (1995). 942
- [35] S. Nakamura, K. Furutaka, H. Wada, T. Fujii, H. Ya- 943
mana, T. Katoh, and H. Harada, Measurement of Ther- 944
mal Neutron Capture Cross Section and Resonance Inte- 945
gral of the $90\text{Sr}(n, \gamma)91\text{Sr}$ Reaction, Journal of Nuclear 946
Science and Technology **38**, 1029 (2001). 947
- [36] C. L. Duncan and K. S. Krane, Neutron capture cross 948
section of 102Pd , Physical Review C **71**, 054322 (2005). 949
- [37] S. Mughabghab, *Thermal Neutron Capture Cross Sec-* 950
tions, Resonance Integrals and G-Factors, Tech. Rep. (In- 951
ternational Atomic Energy Agency, 2003). 952
- [38] A. Y. Dauenhauer and K. S. Krane, Neutron capture 953
cross sections of $130,132,134,136,138\text{Ba}$, Physical Review 954
C **85**, 064301 (2012). 955
- [39] B. Pritychenko and S. F. Mughabghab, Neutron Thermal 956
Cross Sections, Westcott Factors, Resonance Integrals,
Maxwellian Averaged Cross Sections and Astrophysical
Reaction Rates Calculated from the ENDF/B-VII.1,
JEFF-3.1.2, JENDL-4.0, ROSFOND-2010, CENDL-3.1
and EAF-2010 Evaluated Data Librari, Nuclear Data
Sheets **113**, 3120 (2012), arXiv:arXiv:1208.2879v3.
- [40] K. A. Domnanich, E. P. Abel, H. K. Clause, C. Kalman,
W. Walker, and G. W. Severin, An isotope harvest-
ing beam blocker for the National Superconducting Cy-
clotron Laboratory, Nuclear Inst. and Methods in Physics
Research, A **959**, 163526 (2020).
- [41] M. D. Scott, J. Schorp, L. Sutherlin, and J. D. Robertson,
Isotope harvesting with Hollow Fiber Supported Liquid
Membrane (HFSLM), Applied Radiation and Isotopes
157, 109027 (2020).
- [42] M. K. Pandey, H. P. Engelbrecht, J. P. Byrne, A. B.
Packard, and T. R. DeGrado, Production of 89Zr via
the $89\text{Y}(p,n)89\text{Zr}$ reaction in aqueous solution: Effect
of solution composition on in-target chemistry, Nuclear
Medicine and Biology **41**, 309 (2014).
- [43] N. A. Zacchia, D. M. Martinez, and C. Hoehr, Radiolysis
reduction in liquid solution targets for the production of
 89Zr , Applied Radiation and Isotopes **155**, 1 (2020).
- [44] P. E. Koehler, J. L. Ullmann, A. J. Couture, and S. M.
Mosby, Attempting to close the loop on the Oslo tech-
nique at 198Au : Constraining the nuclear spin distri-
bution, in *6th International Workshop on Compound-
Nuclear Reactions and Related Topics* (Berkeley, CA,
2018).